

# Mono-everything: combined limits on dark matter production at colliders from multiple final states

Ning Zhou,<sup>1</sup> David Berge,<sup>2</sup> and Daniel Whiteson<sup>1</sup>

<sup>1</sup>*Department of Physics and Astronomy, University of California, Irvine, CA 92697*

<sup>2</sup>*GRAPPA Institute, University of Amsterdam, Netherlands*

Searches for dark matter production at particle colliders are complementary to direct-detection and indirect-detection experiments, and especially powerful for small masses,  $m_\chi < 100$  GeV. An important collider dark matter signature is due to the production of a pair of these invisible particles with the initial-state radiation of a standard model particle. Currently, collider searches use individual and nearly orthogonal final states to search for initial-state jets, photons or massive gauge bosons. We combine these results across final states and across experiments to give the strongest current collider-based limits in the context of effective field theories, and map these to limits on dark matter interactions with nuclei and to dark matter self-annihilation.

PACS numbers:

1 Though the presence of dark matter in the universe 22  
 2 has been well-established, little is known of its particle 23  
 3 nature or its non-gravitational interactions. A vibrant 24  
 4 experimental program is searching for a weakly interact- 25  
 5 ing massive particle (WIMP), denoted as  $\chi$ , and inter- 26  
 6 actions with standard model particles via some as-yet- 27  
 7 unknown mediator. If the mediator is too heavy to be 28  
 8 resolved, the interaction can be modeled as an effective 29  
 9 field theory with a four-point interaction. 30

10 One critical component of this program is the search 31  
 11 for pair-production of WIMPs at particle colliders, specif- 32  
 12 ically  $pp \rightarrow \chi\bar{\chi}$  at the LHC via some unknown interme- 33  
 13 diate state. As the final state WIMPs are invisible to 34  
 14 the detectors, the events can only be seen if there is as- 35  
 15 sociated initial-state radiation of a standard model par- 36  
 16 ticle [1–3], see Fig 1, recoiling against the dark matter 37  
 17 pair. 38

18 The LHC collaborations have reported limits on the 39  
 19 cross section of  $pp \rightarrow \chi\bar{\chi} + X$  where  $X$  is a gluon or 40  
 20 quark [4, 5], photon [6, 7], and other searches have been 41  
 21 repurposed to study the cases where  $X$  is a  $W$  [8] or  $Z$  42

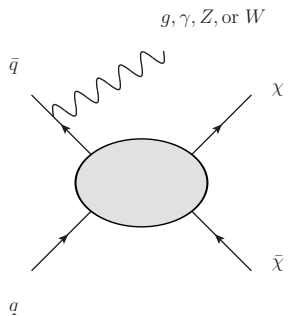


FIG. 1: Pair production of WIMPs ( $\chi\bar{\chi}$ ) in proton-proton collisions at the LHC via an unknown intermediate state, with initial-state radiation of a standard model particle.

boson [9, 10]. In each case, limits are reported in terms of the mass scale  $M_\star$  of the unknown interaction expressed in an effective field theory [1–3, 12–20]. These various initial-state tags probe the same effective theory, but are largely statistically independent due to their nearly orthogonal event selection requirements. As the relative rates of radiation of gluons (quarks), photons,  $W$  or  $Z$  bosons from the incoming quark (gluon) legs are determined by the standard model, the various probes may be combined to give the strongest limits without any loss of generality or additional theoretical assumptions.

Recently, an analysis of multi-jet final states was shown to add some sensitivity to the mono-jet analyses [22]; that sample is not statistically independent from the mono-jet results used here, and is not included. An earlier global analysis of indirect and direct constraints with Tevatron data and mono-jet data from ATLAS provided an initial set of combined constraints [23] using the approximations of a  $\chi^2$  technique.

In this paper, we perform a full statistical combination of the limits from all available channels (mono-jet, mono-photon, mono- $Z^1$  from both ATLAS and CMS at  $\sqrt{s} = 7$  TeV, accounting for the dominant correlations and providing the most powerful current collider constraints. While the limits reported by the experimental collaborations are typically given for a few select effective operators, we calculate the efficiencies of their selections and reinterpret their searches for the complete set of operators relevant for Dirac fermion or complex scalar WIMPs.

## Models

The effective theories of dark matter considered here consider the possibility that the final-state WIMPs are a Dirac fermion (operators D1-D14 in Ref [15]) or a com-

<sup>1</sup> Final states with a heavy boson have little power relative to mono-photon or mono-jet; we include mono- $Z$  as a demonstration, and do not include mono- $W$ , although see [8]. For an alternative view of mono- $Z$ , see Ref [11]

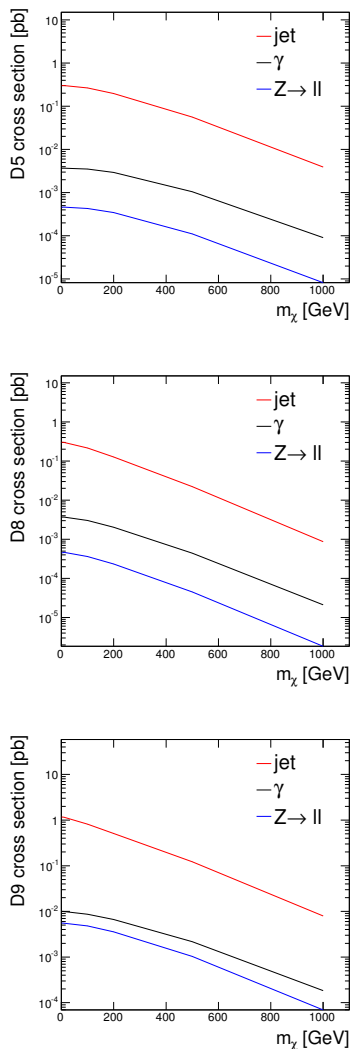


FIG. 2: Cross sections for  $pp \rightarrow \chi\bar{\chi} + X$  production where  $X$  is initial-state radiation of a jet, photon or  $Z$  boson. Jet and photon final states include a  $p_T > 80$  GeV cut at parton-level. Each pane shows the cross section for a different effective operator: top is D5, center is D8, bottom is D9. See Ref. [3] for operator definitions.

plex scalar (operators C1-C6 in Ref [15]). These four-point effective operators assume that the unknown intermediate particles have a heavy mass scale; we use a suppression scale,  $M_*$ . Cross sections at leading order for production in  $pp$  collisions at  $\sqrt{s} = 7$  TeV are shown in Fig 2 for select operators with  $M_* = 1$  TeV for illustration. Recently, next-to-leading-order calculations have been performed for mono-jet and mono-photon processes [24] showing ratios of  $\sigma_{\text{NLO}}/\sigma_{\text{LO}} \approx 1.2 - 1.5$ ; our mono-jet results partially include this effect by generating and matching multiple-parton emission.

For some operators, cross sections of dark matter production at the LHC can be transformed into cross sec-

tions for WIMP-nucleon interaction,  $\sigma(\chi - n)$  [3], or WIMP annihilations [2]. Therefore the effective field theories allow us to map measurements performed at the LHC to the quantities relevant for direct-detection and indirect-detection dark matter search experiments.

The effective-field-theory approach is valid as long as the unknown new mediator particles that couple the dark-matter particles to SM quarks or gluons are too heavy to be resolved:  $q < M_*$ , where  $q$  is the momentum transfer. The breakdown of the effective approach depends ultimately on the details of the new and unknown physics, specifically on the number of new mediator particles and the new couplings. Therefore, these theories cannot be treated generically and must be interpreted with some care. To guide the interpretation, we indicate the range of validity as lower bounds on the mass suppression scale  $M_*$  following ref. [3]. We note that any range of validity of the effective field theory involves assumptions about the unknown physics, see Refs [21] and [22] for additional unitarity arguments and more stringent validity ranges.

Assuming the simplest possible structure of new physics (mediation via exactly one new heavy mediator of mass  $M$ ,  $M_* = M/\sqrt{g_1 g_2}$ ,  $g_1$  and  $g_2$  being coupling constants), bounds on the suppression scale can be placed by requiring  $M > 2m_\chi$  and that the new physics be as strongly coupled as possible for it to be still perturbative ( $\sqrt{g_1 g_2} < 4\pi$ ):

$$M_* > \frac{m_\chi}{2\pi} \text{ (D5 to D14 and C3 to C6),}$$

$$\sqrt{\frac{M_*^3}{m_q}} > \frac{m_\chi}{2\pi} \text{ (D1 to D4),}$$

$$\frac{M_*^2}{m_q} > \frac{m_\chi}{8\pi^2} \text{ (C1 and C2).}$$

Note that we are accounting for additional factors of  $m_q$  in the definitions of operators D1 to D4 and C1, C2 of ref. [3].

## Experimental Searches

The experimental searches typically require one or more high- $p_T$  object and missing transverse momentum, see Table I for a summary and comparison of the mono-photon and mono-jet selections.

The mono- $Z$  analysis [10] uses the ATLAS  $ZZ \rightarrow \ell\nu\nu$  cross-section measurement [9], which requires:

- two same-flavor opposite-sign electrons or muons, each with  $p_T^\ell > 20$  GeV,  $|\eta^\ell| < 2.5$ ;
- dilepton invariant mass close to the  $Z$  boson mass:  $m_{\ell\ell} \in [m_Z - 15, m_Z + 15]$  GeV;
- no particle-level jet with  $p_T^j > 25$  GeV and  $|\eta^j| < 4.5$ ;

TABLE I: Summary of event selection requirements in ATLAS and CMS mono-jet or mono-photon analyses. Note that ATLAS uses two signal regions ( $\cancel{E}_T > 350$  or  $500$  GeV) for the mono-jet analyses, depending on the operator.

	ATLAS	CMS
jet	1 or 2 jets $p_T^{j_1} > 350(500)$ GeV $p_T^{j_2} > 30$ GeV $\cancel{E}_T > 350(500)$ GeV veto leptons $\Delta\phi(j_2, \cancel{E}_T) > 0.5$	1 or 2 jets $p_T^{j_1} > 110$ GeV $p_T^{j_2} > 30$ GeV $\cancel{E}_T > 350$ GeV veto leptons $\Delta\phi(j_1, j_2) < 2.5$
$\gamma$	1 photon, $p_T > 150$ GeV $\cancel{E}_T > 150$ GeV $\leq 1$ jet with $p_T > 30$ GeV isolation details $\Delta\phi(\gamma, \cancel{E}_T) > 0.4$ $\Delta\phi(j_1, \cancel{E}_T) > 0.4$ veto leptons	1 photon $p_T > 145$ GeV $\cancel{E}_T > 130$ GeV 0 track with $p_T > 20$ GeV isolation details

TABLE II: Selection efficiency as percentages for each channel of the analyses used in the combination, for operators D1-14 and C1-C6 for low and high values of the WIMP mass  $m_\chi$ . ATLAS mono-jet analysis has two signal regions, we use  $\cancel{E}_T > 500(350)$  GeV and  $p_T^{j_1} > 500(350)$  GeV region for operators D9-D14 (D1-D8 and C1-C6). Operators D11-14, C5 and C6 only couple to gluon initial states, and so have no efficiency for photon or  $Z$  boson radiation. The  $Z$  efficiencies include the  $Z \rightarrow \ell\ell$  branching fraction. Jet and photon samples include a  $p_T > 80$  GeV cut at parton-level.

Operator	$m_\chi$	ATLAS			CMS	
		jet	$\gamma$	$Z$	jet	$\gamma$
D1	10	0.4%	11.2%	1.2%	0.7%	8.0%
	1000	2.6%	19.1%	1.2%	3.6%	11.3%
D2	10	0.4%	10.8%	1.2%	0.7%	8.0%
	1000	2.4%	18.6%	1.1%	3.7%	11.3%
D3	10	0.5%	11.1%	1.2%	0.7%	8.0%
	1000	2.6%	18.9%	1.2%	3.9%	11.3%
D4	10	0.5%	10.8%	1.2%	0.7%	7.6%
	1000	2.6%	18.6%	1.1%	3.7%	11.3%
D5	10	1.7%	18.2%	0.9%	2.2%	11.3%
	1000	3.3%	23.5%	1.1%	4.5%	14.7%
D6	10	1.7%	18.7%	0.9%	2.2%	12.0%
	1000	3.2%	23.6%	1.1%	4.4%	15.2%
D7	10	1.7%	18.1%	0.9%	2.4%	11.3%
	1000	3.3%	23.4%	1.1%	4.4%	14.5%
D8	10	1.7%	18.5%	0.9%	2.3%	11.8%
	1000	3.1%	23.6%	1.1%	4.3%	15.1%
D9	10	0.9%	23.5%	1.4%	4.1%	14.1%
	1000	1.2%	23.3%	1.4%	5.1%	14.8%
D10	10	1.1%	23.6%	1.4%	4.2%	14.4%
	1000	1.2%	23.4%	1.4%	5.2%	14.8%
D11	10	0.9%	–	–	4.1%	–
	1000	2.4%	–	–	7.5%	–
D12	10	1.0%	–	–	4.2%	–
	1000	2.4%	–	–	7.4%	–
D13	10	0.9%	–	–	4.1%	–
	1000	2.4%	–	–	7.5%	–
D14	10	1.1%	–	–	4.0%	–
	1000	2.4%	–	–	7.4%	–
C1	10	0.1%	7.0%	1.0%	0.2%	5.3%
	1000	2.3%	18.2%	1.1%	3.3%	11.0%
C2	10	0.1%	7.0%	1.0%	0.1%	5.6%
	1000	2.5%	18.4%	1.1%	3.8%	11.2%
C3	10	1.7%	18.4%	0.9%	2.3%	11.6%
	1000	2.9%	23.6%	1.1%	4.1%	14.9%
C4	10	1.4%	18.4%	0.9%	2.2%	11.8%
	1000	3.0%	23.8%	1.1%	4.1%	15.3%
C5	10	1.4%	–	–	1.7%	–
	1000	5.9%	–	–	7.6%	–
C6	10	1.2%	–	–	1.7%	–
	1000	5.9%	–	–	7.6%	–

The backgrounds, their uncertainties and the observed yield can be used to calculate a 90% CL upper limit on the number of signal events  $N$  in the sample, see Table III and Table IV, using the CLs method [25, 26]. This value is almost completely model independent. Translating it into a limit on the cross section for the  $pp \rightarrow \chi\bar{\chi} + X$  sig-

113 •  $(|p_T^{\nu\bar{\nu}} - p_T^Z|)/p_T^Z < 0.6;$

114 •  $-p_T^{\nu\bar{\nu}} \times \cos(\Delta\phi(p_T^{\nu\bar{\nu}}, p_T^Z)) > 80$  GeV.

115 The selection efficiency of each selection for each opera-  
 116 tor is given in Table II and were estimated in the following  
 117 way. References [4–7] provide signal efficiency for several  
 118 select operators; this efficiency is the product of geomet-  
 119 ric and kinematic acceptance of the selection criteria and  
 120 object reconstruction efficiency. The object reconstruction  
 121 efficiency depends on the details of the detector perfor-  
 122 mance, but is largely independent of operator. The  
 123 geometric and kinematic acceptances can be reliably es-  
 124 timated using parton-level simulated event samples. We  
 125 measure the geometric and kinematic efficiency for each  
 126 operator, and use the quoted total efficiencies to deduce  
 127 the object reconstruction efficiencies. This allows us to  
 128 estimate the total efficiency for each operator.

### 129 Combination

130 The separate analyses, each of which are single-bin  
 131 counting experiments, are combined into a multi-bin  
 132 counting experiment. This allows for a coherent signal  
 133 rate to be tested across channels, but preserves their dis-  
 134 tinct signal-to-background ratios.

135 The background estimates are taken directly from the  
 136 experimental publications, see a summary in Table III,  
 137 and are assumed to be uncorrelated across channels,  
 138 as they are typically dominated by channel-specific or  
 139 detector-specific uncertainties. For example, in some  
 140 cases the background estimates are data-driven, and the  
 141 dominant uncertainties are in the finite statistics of in-  
 142 dependent control samples. Inclusion of correlations up  
 143 to 20% does not qualitatively impact the results of the  
 144 combination.

TABLE III: 90% CL limits on  $N_{\text{events}}$ , efficiencies for  $m_\chi = 10$  GeV, and limits on  $\sigma(pp \rightarrow \chi\bar{\chi} + X)$  using the D5 operator. In the case of the  $Z + \cancel{E}_T$  final state, the efficiency is relative to  $Z \rightarrow \ell\ell$  decays only.

Channel	Bg.	Obs	Limit	Eff.	Lumi.	Limit
		$N$	$N$	(%)	( $\text{fb}^{-1}$ )	$\sigma$ (fb)
ATLAS jet+ $\cancel{E}_T$	$750 \pm 60$	785	139.3	1.7%	4.8	1,700
CMS jet+ $\cancel{E}_T$	$1225 \pm 101$	1142	125.2	2.2%	5.0	1,140
ATLAS $\gamma + \cancel{E}_T$	$137 \pm 20$	116	27.4	18%	4.6	33
CMS $\gamma + \cancel{E}_T$	$75.1 \pm 9.4$	73	19.3	11%	5.0	35
ATLAS $Z + \cancel{E}_T$	$86.2 \pm 7.2$	87	21.7	13%	4.6	36

TABLE IV: 90% CL limits on  $N_{\text{events}}$ , efficiencies for  $m_\chi = 10$  GeV, and limits on  $\sigma(pp \rightarrow \chi\bar{\chi} + X)$  using the D9 operator.

Channel	Bg.	Obs	Limit	Eff.	Lumi.	Limit
		$N$	$N$	(%)	( $\text{fb}^{-1}$ )	$\sigma$ (fb)
ATLAS jet+ $\cancel{E}_T$	$83 \pm 14$	77	25.5	0.9%	4.8	590
CMS jet+ $\cancel{E}_T$	$1225 \pm 101$	1142	125.2	4.1%	5.0	610

nal requires the efficiency of the signal in each selection, see Table III. These individual limits reproduce well the results reported by the experiments.

The signal regions are nearly orthogonal, but not exactly. For example, the mono-jet analyses do not veto events with a photon, and the mono-photon analyses allow the presence of one jet. From our parton-level simulated event samples, we estimated the overlaps among different channels and found that the overlap fraction is less than 1%.

The individual analyses include signal uncertainties of up to 20% on the cross section, mostly due to uncertainties in jet energy calibration and levels of initial-state radiation. These uncertainties do not affect the cross-section limits, but can be simply applied to limits on  $M_\star$ . In each case, we quote the limit using the central value.

To summarize, the assumptions made in this combination are

- the background uncertainties are monolithic and uncorrelated, and
- the signal selections are orthogonal

Combining channels is then straightforward, though the intermediate step of a model-independent limit on the number of events  $N$  is no longer possible, as the limits depend on the relative distribution of signal events across channels, which is model specific. Instead, cross-section limits are obtained directly. These limits are then converted into limits on  $M_\star$ , using the relationships from Ref. [15]. The individual-channel limits, combination across experiments and the grand combination of all channels are shown in Table V for the D5 operator and one choice of  $m_\chi$ . Clearly the mono-jet analyses are the most powerful, and the greatest gain in combination is

TABLE V: 90% CL limits on  $\sigma(pp \rightarrow \chi\bar{\chi} + X)$  for  $m_\chi = 10$  GeV, theory prediction for  $M_\star = 1$  TeV, and limits on  $M_\star$  using the D5 operator. In the case of the  $Z + \cancel{E}_T$  final state, the predictions include the  $Z \rightarrow \ell\ell$  branching fraction.

Channel	Limit $\sigma$	Pred.	Limit $M_\star$	
	(fb)	(fb)	(GeV)	
ATLAS jet+ $\cancel{E}_T$	1,700	370	685	} 785
CMS jet+ $\cancel{E}_T$	1,140	370	750	
ATLAS $\gamma + \cancel{E}_T$	33	3.7	580	} 645 } 795
CMS $\gamma + \cancel{E}_T$	35	3.7	570	
ATLAS $Z + \cancel{E}_T$	36	0.5	340	

from combining the ATLAS and CMS mono-jet analyses, though the addition of the mono-photon and mono- $Z$  gives a non-negligible improvement in the combined result.

Limits on  $M_\star$  for the D5 and D8 operators are shown in Fig 3 and 4, as well as limits on  $\sigma(\chi - n)$ . Where the  $M_\star$  limits exceed the thermal relic values taken from Ref. [3], assuming that dark matter is entirely composed of thermal relics, the resulting dark matter density of the universe would contradict WMAP measurements; therefore, WIMPs cannot couple to quarks or gluons exclusively via the given operator and account entirely for the relic density. This  $m_\chi$  region is either excluded, or requires that annihilation channels to leptons must exist, or participation of different operators which interfere negatively, thereby reducing the limits on  $M_\star$ .

### Application to other models

While the experimental results are usually quoted for a small selection of the effective operator models, the analyses are clearly relevant for all of them.

We re-interpret the experimental analyses in the context of each operator and perform the grand combination across all channels. Figure 5 and Table VI show the limits on  $M_\star$ , translated to the WIMP-nucleon cross section where possible. In addition, we translate the limits on D5 and D8 into limits on the WIMP annihilation cross section, see Fig. 6.

### Conclusions

We have presented the first combination of collider-based searches for dark matter pair production, using final states involving jets, photons and leptonically-decaying  $Z$  bosons in the context of effective field theories. The most powerful results are from the mono-jet analyses, and the greatest gains come from the combination of the independent analyses from ATLAS and CMS, though the other final states make a non-negligible improvement. The results are the strongest limits to date

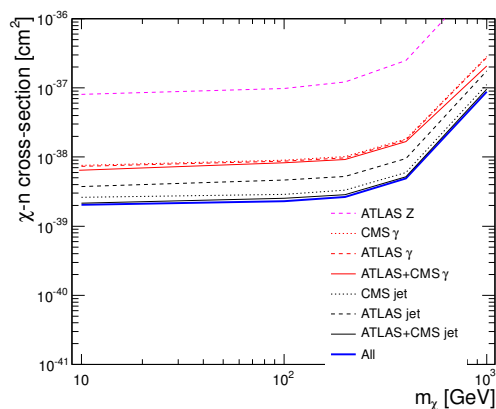
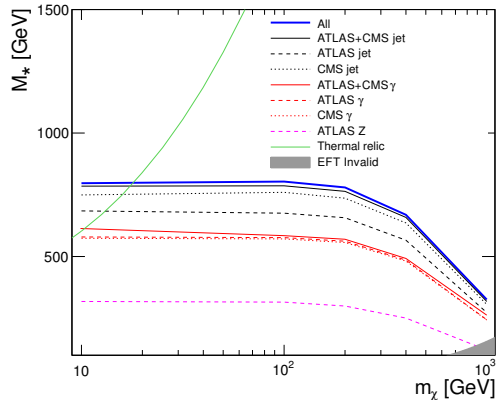


FIG. 3: Limits at 90% CL in  $M_*$  (top) and in the spin-independent WIMP-nucleon cross section (bottom) for individual and combined limits using the D5 operator as a function of  $m_\chi$ .

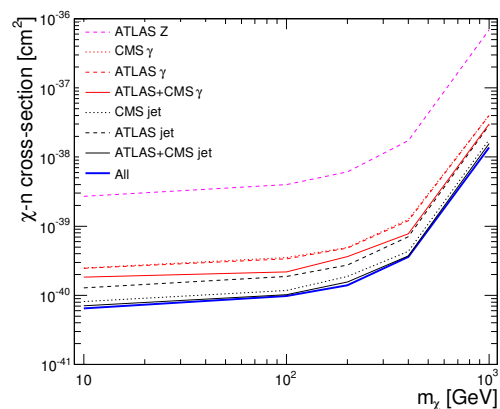
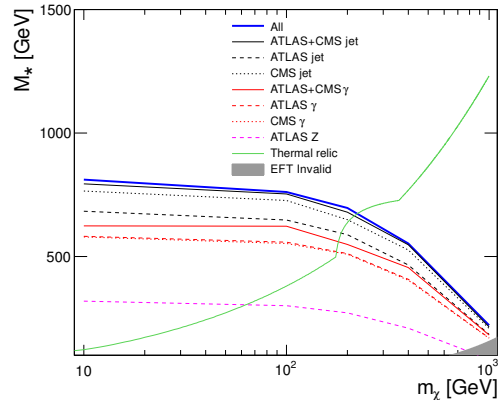


FIG. 4: Limits at 90% CL in  $M_*$  (top) and in the spin-independent WIMP-nucleon cross section (bottom) for individual and combined limits using the D8 operator as a function of  $m_\chi$ .

236

### Acknowledgements

We acknowledge useful conversations with Tim Tait, Roni Harnik and Patrick Fox. DW and NZ are supported by grants from the Department of Energy Office of Science and by the Alfred P. Sloan Foundation.

- 
- [1] M. Beltran, D. Hooper, E. W. Kolb, Z. A. C. Krusberg and T. M. P. Tait, *JHEP* **1009**, 037 (2010) [arXiv:1002.4137 [hep-ph]].
  - [2] P. J. Fox, R. Harnik, J. Kopp and Y. Tsai, *Phys. Rev. D* **85**, 056011 (2012) [arXiv:1109.4398 [hep-ph]].
  - [3] J. Goodman, M. Ibe, A. Rajaraman, W. Shepherd, T. M. P. Tait and H. -B. Yu, *Phys. Rev. D* **82**, 116010 (2010) [arXiv:1008.1783 [hep-ph]].
  - [4] G. Aad *et al.* [ATLAS Collaboration], arXiv:1210.4491 [hep-ex].
  - [5] S. Chatrchyan *et al.* [CMS Collaboration], *JHEP* **1209**,

222 from collider searches in the effective field theory context. 237

223 In addition, we have reinterpreted the experimental re- 238  
 224 sults, quoted by ATLAS and CMS only for a few effective 239  
 225 operators, across a broad range of operators, providing 240  
 226 a comprehensive view of the power of these searches to 241  
 227 constrain the weak-level or weaker interactions between 242  
 228 dark matter and standard model particles. 243

229 We have made use of the effective field theory frame- 244  
 230 work to convert the ATLAS and CMS results to quan- 245  
 231 tities relevant for direct-detection and indirect-detection 246  
 232 dark matter searches. Under the assumptions made for 247  
 233 the effective operators, LHC limits can be very compet- 248  
 234 itive, in particular for low-mass dark matter particles 249  
 235  $m_\chi \leq 10$  GeV. 250  
 251

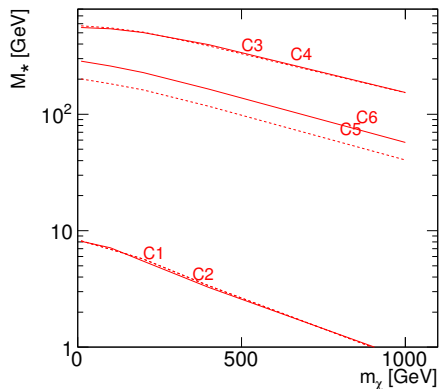
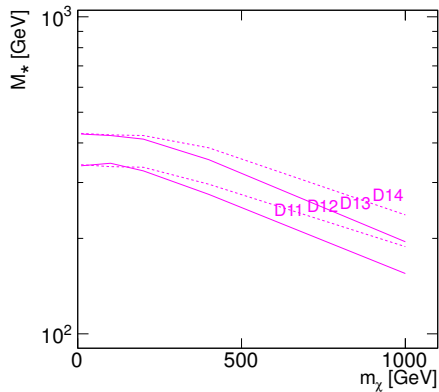
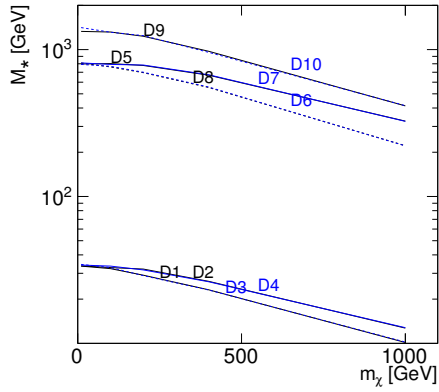


FIG. 5: Combined limits on  $M_*$  at 90% CL, using all available channels, for operators D1-14 and C1-C5 as a function of  $m_\chi$ .

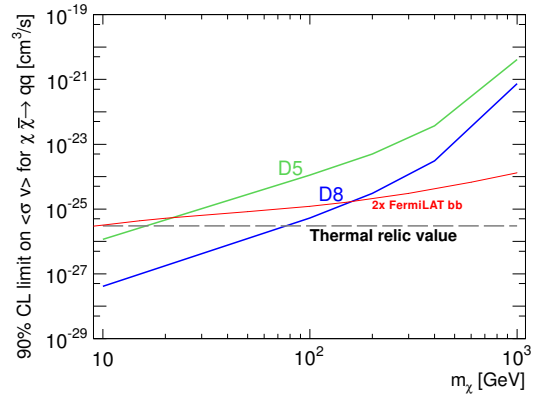
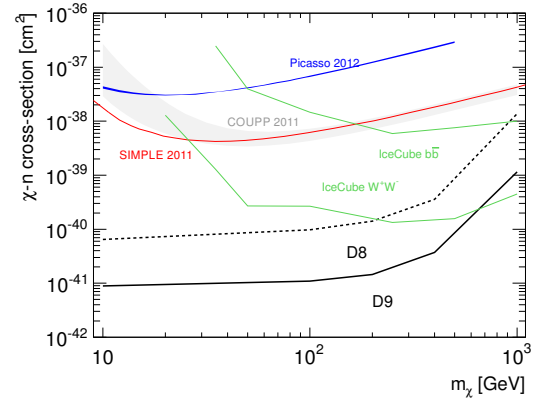
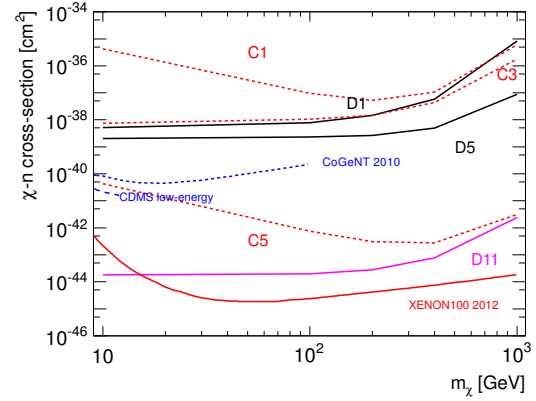


FIG. 6: Top and center, limits at 90% CL on the spin-independent and spin-dependent WIMP-nucleon cross section,  $\sigma(\chi-n)$ , for available operators. Bottom, interpretation of the limits on D5 and D8 in terms of the velocity-averaged WIMP-annihilation cross section, as defined in Ref [2].

252 094 (2012) [arXiv:1206.5663 [hep-ex]]. 261  
 253 [6] G. Aad *et al.* [ATLAS Collaboration], arXiv:1209.4625 262  
 254 [hep-ex]. 263  
 255 [7] S. Chatrchyan *et al.* [CMS Collaboration], Phys. Rev. 264  
 256 Lett. **108**, 261803 (2012) [arXiv:1204.0821 [hep-ex]]. 265  
 257 [8] Y. Bai and T. M. P. Tait, arXiv:1208.4361 [hep-ph]. 266  
 258 [9] G. Aad *et al.* [ATLAS Collaboration], arXiv:1211.6096 267  
 259 [hep-ex]. 268  
 260 [10] L. M. Carpenter, A. Nelson, C. Shimmin, T. M. P. Tait 269

and D. Whiteson, arXiv:1212.3352 [hep-ex].  
 [11] N. F. Bell, J. B. Dent, A. J. Galea, T. D. Jacques,  
 L. M. Krauss and T. J. Weiler, Phys. Rev. D **86**, 096011  
 (2012) [arXiv:1209.0231 [hep-ph]].  
 [12] M. Beltran, D. Hooper, E. W. Kolb and Z. C. Krusberg,  
 Phys. Rev. D **80**, 043509 (2009) [arXiv:0808.3384 [hep-  
 ph]].  
 [13] W. Shepherd, T. M. P. Tait and G. Zaharijas, Phys. Rev.  
 D **79**, 055022 (2009) [arXiv:0901.2125 [hep-ph]].

TABLE VI: Combined limits on  $M_*$  at 90% CL, using all available channels, for operators D1-11 and C1-C5 for low and high values of the WIMP mass  $m_\chi$ . Where possible, limits are shown on the WIMP-nucleon cross section,  $\sigma(\chi - n)$ .

Operator	$m_\chi$ (GeV)	$M_*$ (GeV)	$\sigma(\chi - n)$ [cm <sup>2</sup> ]
D1	10	34	$5.2 \times 10^{-39}$
	1000	10	$8.3 \times 10^{-36}$
D2	10	34	
	1000	13	
D3	10	34	
	1000	10	
D4	10	34	
	1000	13	
D5	10	795	$2.0 \times 10^{-39}$
	1000	325	$8.8 \times 10^{-38}$
D6	10	791	
	1000	221	
D7	10	812	
	1000	324	
D8	10	811	$6.5 \times 10^{-41}$
	1000	222	$1.4 \times 10^{-38}$
D9	10	1331	$8.9 \times 10^{-42}$
	1000	413	$1.1 \times 10^{-39}$
D10	10	1410	
	1000	415	
D11	10	339	$1.8 \times 10^{-44}$
	1000	155	$2.4 \times 10^{-42}$
D12	10	342	
	1000	188	
D13	10	427	
	1000	195	
D14	10	429	
	1000	237	
C1	10	8	$4.2 \times 10^{-36}$
	1000	1	$6.1 \times 10^{-36}$
C2	10	8	
	1000	1	
C3	10	575	$7.5 \times 10^{-39}$
	1000	153	$1.8 \times 10^{-36}$
C4	10	556	
	1000	154	
C5	10	201	$4.4 \times 10^{-41}$
	1000	41	$3.1 \times 10^{-42}$
C6	10	286	
	1000	57	

- [14] Q. -H. Cao, C. -R. Chen, C. S. Li and H. Zhang, JHEP **1108**, 018 (2011) [arXiv:0912.4511 [hep-ph]].
- [15] J. Goodman, M. Ibe, A. Rajaraman, W. Shepherd, T. M. P. Tait and H. -B. Yu, Phys. Lett. B **695**, 185 (2011) [arXiv:1005.1286 [hep-ph]].
- [16] Y. Bai, P. J. Fox and R. Harnik, JHEP **1012**, 048 (2010) [arXiv:1005.3797 [hep-ph]].
- [17] A. Rajaraman, W. Shepherd, T. M. P. Tait and A. M. Wijangco, Phys. Rev. D **84**, 095013 (2011) [arXiv:1108.1196 [hep-ph]].
- [18] R. C. Cotta, J. L. Hewett, M. P. Le and T. G. Rizzo, arXiv:1210.0525 [hep-ph].
- [19] F. J. Petriello, S. Quackenbush and K. M. Zurek, Phys.

- Rev. D **77**, 115020 (2008) [arXiv:0803.4005 [hep-ph]].
- [20] Y. Gershtein, F. Petriello, S. Quackenbush and K. M. Zurek, Phys. Rev. D **78**, 095002 (2008) [arXiv:0809.2849 [hep-ph]].
- [21] I. M. Shoemaker, L. Vecchi and , Phys. Rev. D **86**, 015023 (2012) [arXiv:1112.5457 [hep-ph]].
- [22] P. J. Fox, R. Harnik, R. Primulando and C. -T. Yu, Phys. Rev. D **86**, 015010 (2012) [arXiv:1203.1662 [hep-ph]].
- [23] K. Cheung, P. -Y. Tseng, Y. -L. S. Tsai and T. -C. Yuan, JCAP **1205**, 001 (2012) [arXiv:1201.3402 [hep-ph]].
- [24] P. J. Fox and C. Williams, arXiv:1211.6390 [hep-ph].
- [25] A. Read, J. Phys. G: Nucl. Part. Phys. **28**, 2693 (2002);
- [26] T. Junk, Nucl. Instrum. Methods A **434**, 425 (1999).
- [27] J. Alwall, M. Herquet, F. Maltoni, O. Mattelaer and T. Stelzer, JHEP **1106**, 128 (2011) [arXiv:1106.0522 [hep-ph]].

## Appendix: Individual Operators

299

300

301

302

303

304

In Figs. 7, 8, 9, 10 11, and 12 we show the combined limits for each operator, compared to the thermal relic values. Where the limits exceed the thermal relic values, assuming that dark matter is entirely composed of thermal relics, the dark matter density of the universe

305

306

would contradict measurements and hence cannot couple to quarks or gluons exclusively via the given operator. This  $m_\chi$  region is either excluded, or else other annihilation channels to leptons must exist, or finally different operators may interfere negatively thereby reducing the limits on  $M_\star$ .



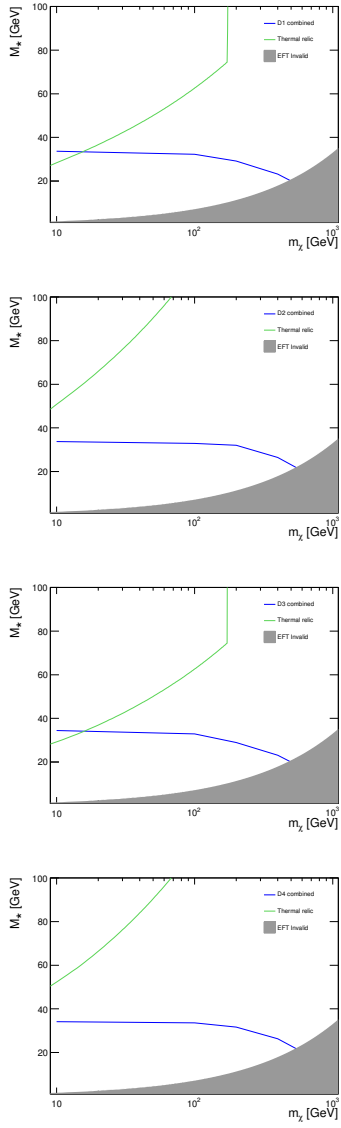


FIG. 7: Combined limits on  $M_*$  versus dark matter mass  $m_\chi$  for operators D1, D2, D3 and D4. The  $M_*$  values at which dark matter particles of a given mass would result in the required relic abundance are shown as green lines [3], assuming annihilation in the early universe proceeded exclusively via the given operator.

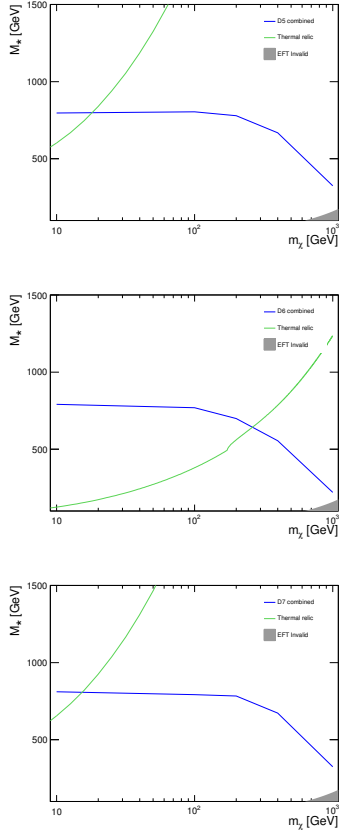


FIG. 8: Combined limits on  $M_*$  versus dark matter mass  $m_\chi$  for operators D5, D6, and D7. The  $M_*$  values at which dark matter particles of a given mass would result in the required relic abundance are shown as green lines [3], assuming annihilation in the early universe proceeded exclusively via the given operator.

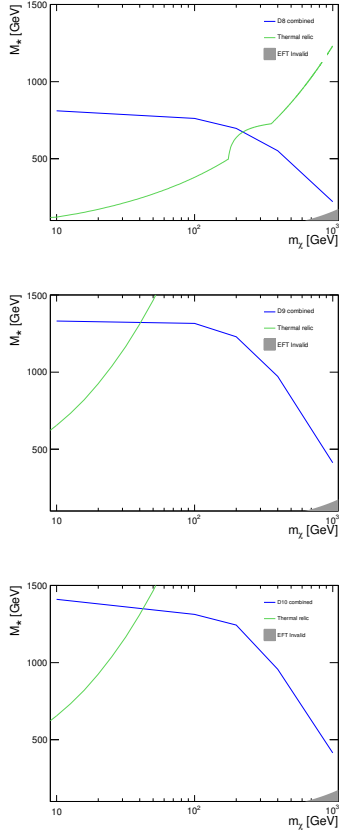


FIG. 9: Combined limits on  $M_*$  versus dark matter mass  $m_\chi$  for operators D8, D9 and D10. The  $M_*$  values at which dark matter particles of a given mass would result in the required relic abundance are shown as green lines [3], assuming annihilation in the early universe proceeded exclusively via the given operator.

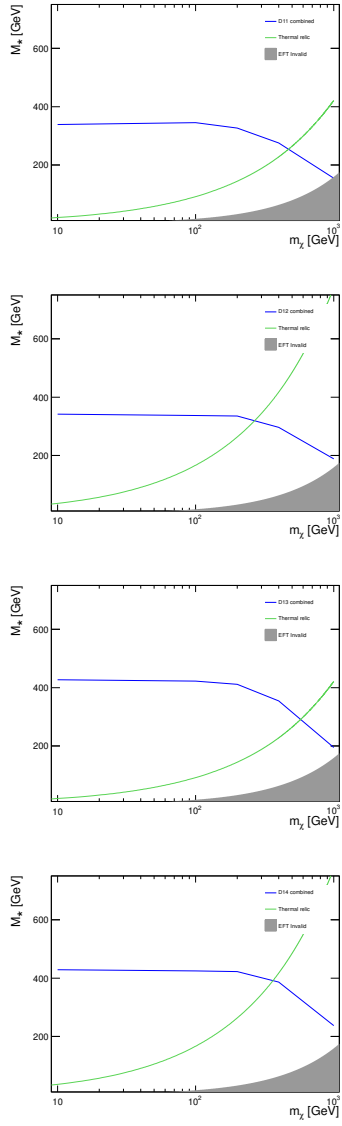


FIG. 10: Combined limits on  $M_*$  versus dark matter mass  $m_\chi$  for operators D11, D12, D13 and D14. The  $M_*$  values at which dark matter particles of a given mass would result in the required relic abundance are shown as green lines [3], assuming annihilation in the early universe proceeded exclusively via the given operator.

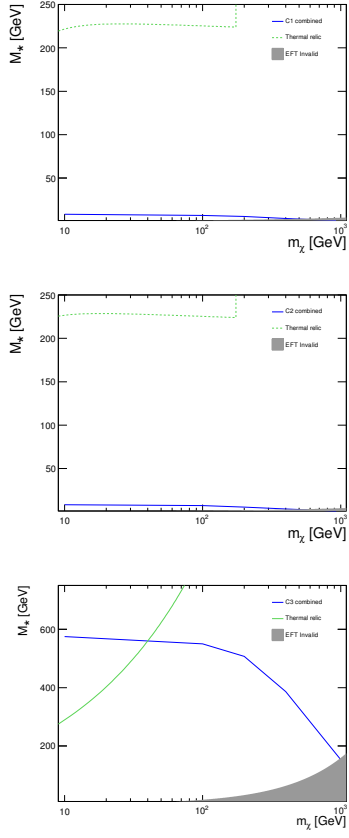


FIG. 11: Combined limits on  $M_*$  versus dark matter mass  $m_\chi$  for operators C1, C2, and C3. The  $M_*$  values at which dark matter particles of a given mass would result in the required relic abundance are shown as green lines [3], assuming annihilation in the early universe proceeded exclusively via the given operator.

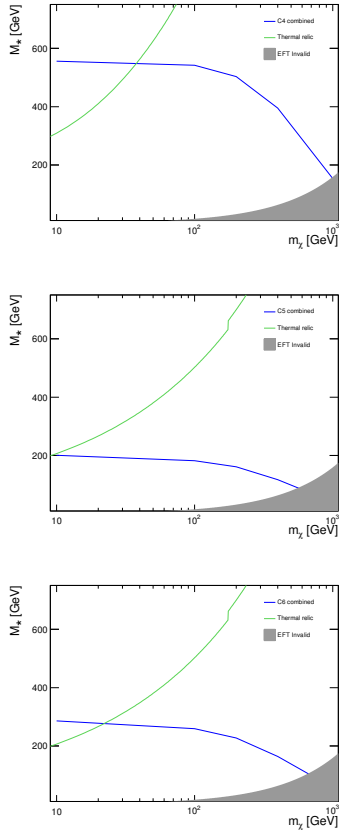


FIG. 12: Combined limits on  $M_*$  versus dark matter mass  $m_\chi$  for operators C4, C5 and C6. The  $M_*$  values at which dark matter particles of a given mass would result in the required relic abundance are shown as green lines [3], assuming annihilation in the early universe proceeded exclusively via the given operator.